Nano Energy 102 (2022) 107654

Contents lists available at ScienceDirect

Nano Energy

journal homepage: www.elsevier.com/locate/nanoen

Atomic-scale insights into the role of non-covalent interactions in electrocatalytic hydrogen evolution reaction

Zhaoyan Luo [a,b,d], Lei Zhang [a], Lei Wu [a], Lei Wang [c], Qianling Zhang [a,b,c,d], Xiangzhong Ren [a,*], Xueliang Sun [d,*]

[a] College of Chemistry and Environmental Engineering, Shenzhen University, Shenzhen, Guangdong 518060, PR China
[b] College of Physics and Optoelectronic Engineering, Shenzhen University, Shenzhen, Guangdong 518060, PR China
[c] College of Materials science And Engineering, Shenzhen University, Shenzhen, Guangdong 518060, PR China
[d] Department of Mechanical and Materials Engineering, University of Western Ontario, 1151 Richmond St, London, Ontario N6A 3K7, Canada

ARTICLE INFO

Keywords:
Non-covalent interactions
Model catalyst surface
Hydrogen evolution reaction
Electron-withdrawing
Interface engineering

ABSTRACT

Understanding the non-covalent interactions occurring at electrocatalytic interfaces is important to promote the development of advanced hydrogen evolution systems. However, the exact role of non-covalent interaction in the electrode–electrolyte interface on the HER kinetics remains obscure at the molecular level, especially for non-platinum-based electrodes. This is due to the lack of an effective strategy to decouple the effect of each interaction (ΔG_H, noncovalent interactions) on the HER kinetics. Accordingly, herein, we constructed a model catalyst surface (Pd,$RuSO_y$) to decouple the influence of ΔG_H and double-layer structure optimization on HER kinetics, thus exploring the role of this non-covalent interactions on the HER at the molecular level. We found that hydrated cations located in the outer Helmholtz plane (OHP) also interact directly with electrode materials and the strength of these interactions would also affect the HER activity. Consequently, Pd,$RuS_{2-x}O_y$ exhibited remarkable electrocatalytic activity toward HER, which delivered low overpotentials of 38 and 82 mV at 10 and 100 mA cm^{-2}, respectively. This study not only illustrates the roles of interfacial interactions, but also provides a new way for the rational design of advanced electrocatalysts.

1. Introduction

Renewable-powered, low-temperature water electrolyzers are significantly important alternatives to fossil fuels for green hydrogen production [1–3]. Developing cost-effective Pt group metal (PGM)-free catalysts for hydrogen evolution reaction (HER) is the key to realizing the large-scale application of proton exchange membrane water electrolyzers (PEMWEs) [4,5]. Persistent research efforts have uncovered that a well-known correlation exists between the HER activity and the binding strength of H (ΔG_H) on the catalyst surface, which follows a 'volcano' trend (Sabatier principle) [6–9]. Numerous studies have thus been performed on enhancing the HER performance of catalysts by optimizing the energy of the reaction intermediates (H*) on the surface of catalysts [10–12]. Although certain success has been achieved in this regard, important kinetic details have been overlooked, and accordingly, huge disparity exists between the performances of different catalysts located at the apex of the volcano plot [13–18]. In addition, ΔG_H fail to capture the influence of external parameters (such as pH or the presence of Li^+ cations in the electrolyte) on HER activity. These issues stem from the fact that: in aqueous electrolytes, the catalytic properties not only depend on the energetics of interactions between key reaction intermediates and catalyst surface(ΔG_H), but are also governed by the non-covalent interactions between electrode surfaces and hydronium ions (H_3O^+)/water molecules in the electrochemical double-layer (EDL). However, our understanding of the impact of weak interactions in electrode interface on the HER kinetics remains elusive at the molecular level.

One key challenge for exploring the role of non-covalent interactions in electrocatalytic hydrogen evolution reactions on electrode interface is the lack of an effective strategy to decouple the effect of the two types of interactions (ΔG_H, noncovalent interactions) on the HER reaction kinetics. For instance, our previous study [19] has revealed that the introduction of -OH group into MoS_2 via Pd,Ru-doping strategy can endow the interface with reactant dragging functionality. Meanwhile, in-plane inert sulfur sites are also electronically activated by heteroatom metal doping (Pd and Ru) to acquire optimized hydrogen adsorption

* Corresponding authors.
E-mail addresses: renxz@szu.edu.cn (X. Ren), xsun9@uwo.ca (X. Sun).

https://doi.org/10.1016/j.nanoen.2022.107654
Received 5 November 2021; Received in revised form 27 April 2022; Accepted 29 July 2022
Available online 30 July 2022

energy. Therefore, in order to draw this molecular understanding for the dependence of the HER on the EDL structure, we must first develop model catalytic surface to decouple the effect of the two types of interactions on the reaction kinetics.

Considering that the electron-withdrawing O sites can form H bonds with H_3O^+ or H_2O on the EDL, O doping can be expected to induce interface engineering. Furthermore, a previous study [20] has revealed that the chemisorption of O on chalcogen atoms has a relatively weak influence on the band structure and geometry configuration of transition metal dichalcogenides (TMDs); thus, this O-doped TMDs surface may decouple the effect of the two types of interactions on the reaction kinetics, thereby helping us to the understand the importance of non-covalent interactions in controlling the catalytic activity during HER.

Herein, we created a model catalyst surface (Pd,$RuS_{2-x}O_y$) by spontaneously incorporating O atoms into ruthenium disulfide (RuS_2) lattices. Pd,$RuS_{2-x}O_y$ comprised sites of optimum H* binding strength, which also formed a hydrogen-bonding network with H_3O^+ or H_2O in the electrolyte. More attractively, the model catalyst surface decoupled the influence of ΔG_H and double-layer structure optimization on HER kinetics. Specifically, our study highlights that by achieving control over the non-covalent interactions between the electrode surface and hydrated cations located in the outer Helmholtz plane (OHP), electrocatalytic activity at electrified interfaces can be tuned. Correspondingly, a significant enhancement in the HER performance of Pd,$RuS_{2-x}O_y$ was realized (Overpotential: 82 mV at 100 mA cm^{-2} and Tafel slope: 62 mV dec^{-1} in high current density regions), exceeding the HER performances of most of the existing PGM-free catalysts in acidic environments. This work may provide a way to unleash the electrocatalytic potential of TMD materials for efficient hydrogen generation in acidic media.

2. Results and discussion

2.1. Design model catalyst surface

Structurally, the substitution of O for S in the RuS_2 lattice is conducted to prepare a model catalyst surface. However, realizing O substitution on the defect-free basal plane without altering the phase structure remains a considerable challenge [8,20]. Based on our previous studies [8,21], herein, we substituted S sites by O sites via a surface redox reaction with Pd. Pd interfacial doping can create structural vacancies on the RuS_2 surface, thus making the introduction of O thermodynamically favorable. To investigate the thermodynamics of the introduction of O atoms into RuS_2 crystals by Pd doping, we performed density functional theory (DFT) calculations. At first, we calculated the formation energy of sulfur vacancies (SVs) in RuS_2 and Pd–RuS_2, which was decreased by ~1 eV due to Pd doping (Fig. 1a). Then, we evaluated the adsorption energies of the O-containing species on SVs and found that the chemisorption of O atoms on the SV site of RuS_2 was exothermic (Fig. 1b-e and Fig. S1). In contrast, the chemisorption of other species (namely, -OH at 0.81–1.61 eV and O_2 at 3.2–3.5 eV) to saturate the SVs was thermodynamically unfavorable. Furthermore, the higher strength of Ru–O bonds as compared to that of Ru–S bonds [20] also facilitated the capture of nucleophilic O species by the SV sites.

Based on the predicted structure of Pd,$RuS_{2-x}O_y$, we synthesized Pd, $RuS_{2-x}O_y$, and the synthetic procedures are illustrated in Fig. S2. The structure of Pd,$RuS_{2-x}O_y$ was examined by transmission electron microscopy (TEM), X-ray diffraction (XRD), and sub-angstrom resolution aberration-corrected high-angle annular dark field–scanning transmission electron microscopy (HAADF–STEM). TEM images showed that the introduction of Pd did not induce noticeable morphological changes in RuS_2 (Fig. 2a and Fig. S3). Moreover, no Pd particles or clusters were observed in the TEM image, thus excluding the possibility of the formation of phase-segregated Pd or Pd sulfide (PdS) compounds. To exclude the possibility of the formation of the amorphous PdS, the Pd, $RuS_{2-x}O_y$ sample after heat-treatment at 600 °C further characterized by XRD (Fig. 2b). The result reveals that Pd was firmly integrated into the RuS_2 backbone without phase segregation, which also indicated the absence of the amorphous PdS. Furthermore, the high-resolution Pd 3d XPS spectrum was deconvoluted into two peaks that were assigned to Pd $3d_{5/2}$ (336.7 eV) and Pd $3d_{3/2}$ (342 eV) (Fig. 2c), which implied that Pd was immobilized as Pd (II) in the RuS_2 backbone. Atomic-resolution aberration-corrected HAADF–STEM was used to examine the structure of Pd,$RuS_{2-x}O_y$. The HAADF–STEM images and corresponding

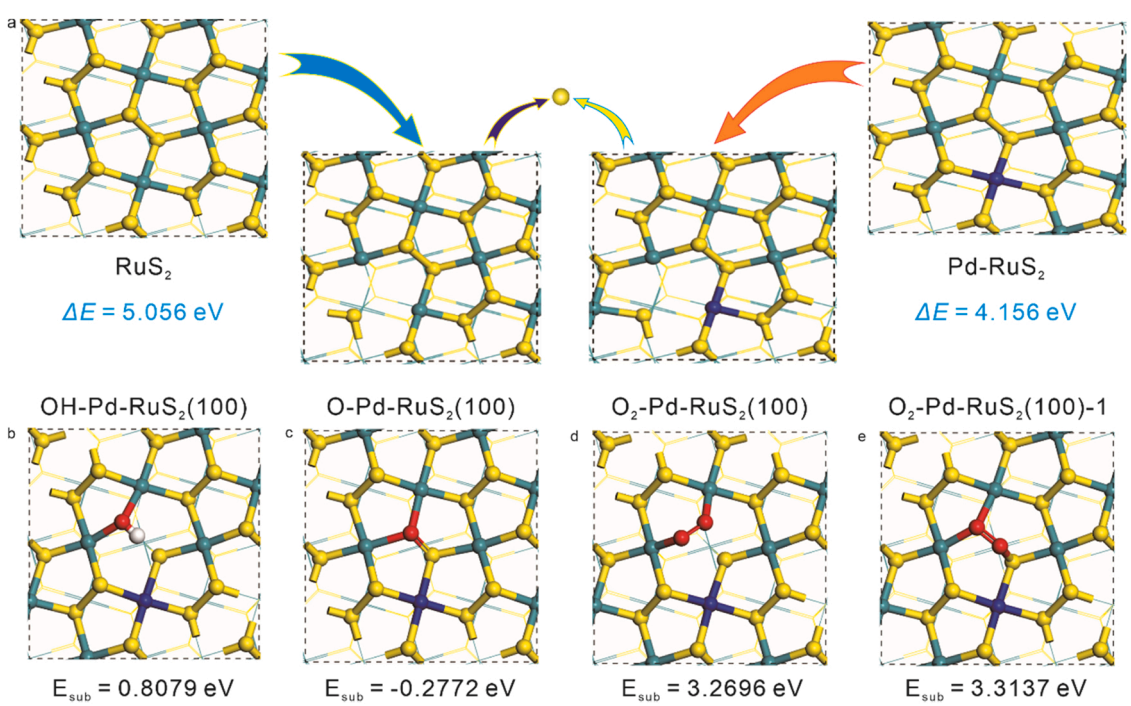

Fig. 1. (a) Formation of sulfur vacancies in RuS_2 and Pd-RuS_2. (b) Formation energies of OH occupying the sulfur defect sites in RuS_2. (c) Formation energies of O occupying the sulfur defects sites in RuS_2. (d) and (e) Formation energies of O_2 occupying the sulfur defects sites in RuS_2.

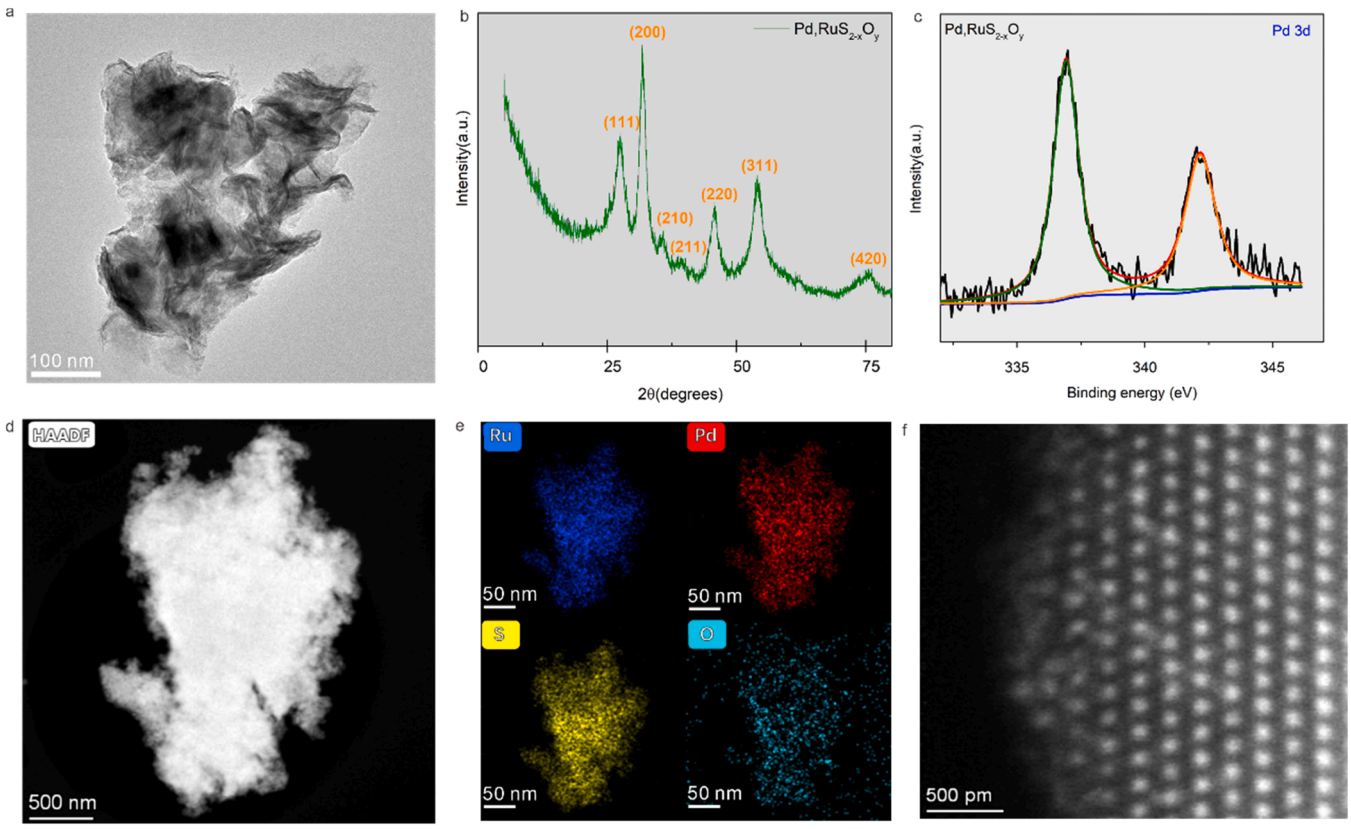

Fig. 2. (a) Transmission electron microscopy image of $Pd,RuS_{2-x}O_y$. (b) X-ray diffraction pattern of $Pd,RuS_{2-x}O_y$ sample after heat-treatment at 600 °C. (c) High-resolution Pd 3d X-ray photoelectron spectrum of $Pd,RuS_{2-x}O_y$. (d-e) High-angle annular dark field–scanning transmission electron microscopy (HAADF–STEM) image and corresponding elemental mapping of Pd, Ru, O, and S, respectively. (f) Atomic-resolution HAADF–STEM image of $Pd,RuS_{2-x}O_y$.

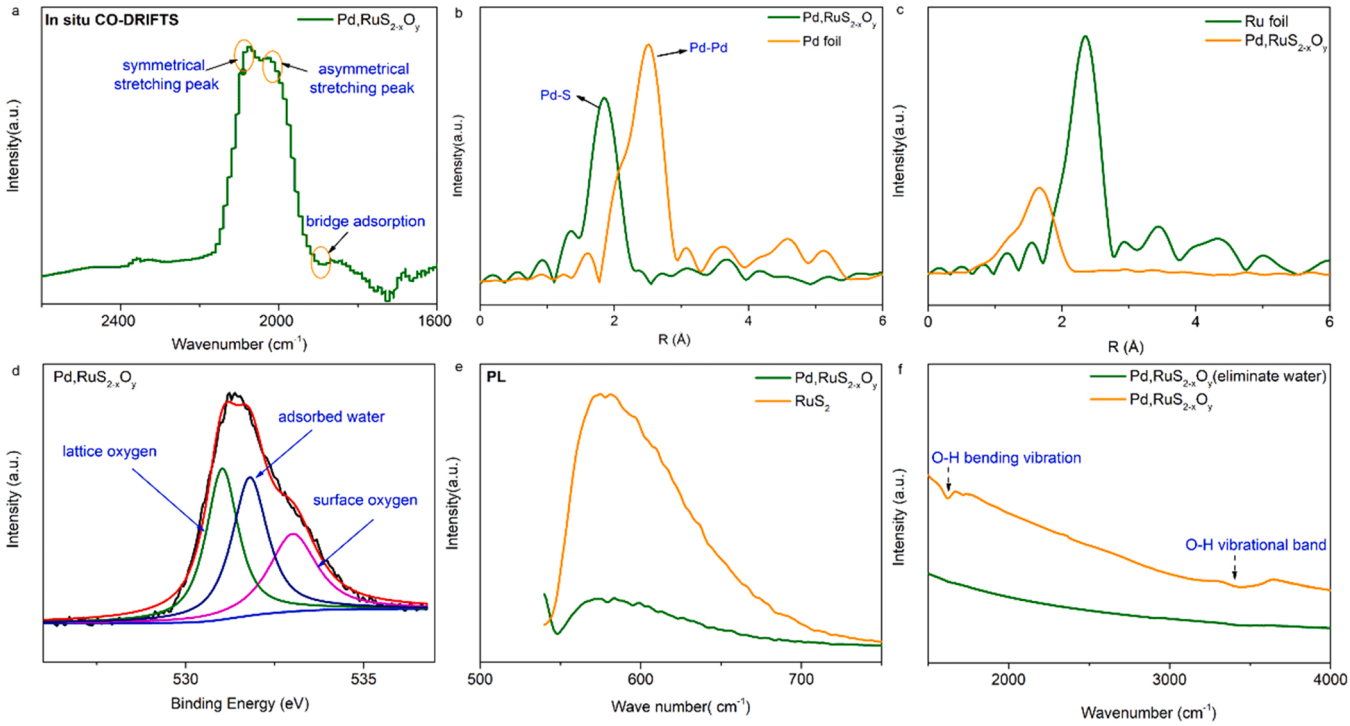

Fig. 3. (a) In situ diffuse reflectance infrared Fourier transform spectra of $Pd,RuS_{2-x}O_y$ acquired using CO as a probe molecule. (b) Fourier transform of the k^2-weighted Pd K-edge extended X-ray absorption fine structure (EXAFS) spectra. (c) Fourier transform of the k^2-weighted Ru K-edge EXAFS spectra. (d) X-ray photoelectron spectra of $Pd,RuS_{2-x}O_y$. (e) Photoluminescence spectra of RuS_2 and $Pd,RuS_{2-x}O_y$. (f) Fourier transform infrared spectra of $Pd,RuS_{2-x}O_y$.

elemental mappings of Pd,$RuS_{2-x}O_y$ revealed that the Pd atoms were homogeneously distributed and atomically confined into the RuS_2 lattice (Fig. 2d-f). This finding was verified by in situ diffuse reflectance infrared Fourier transform spectroscopy using CO as a probe molecule. In the spectrum of CO adsorbed-Pd,$RuS_{2-x}O_y$, a broad peak at 1870 cm^{-2} attributed to the bridge configurations of the CO molecules adsorbed on Pd was barely observable (Fig. 3a), indicating that the Pd species were not in the form of metallic Pd nanoparticles or clusters. Instead, the infrared absorption peaks generally associated with the symmetric and asymmetrical stretching of CO adsorption on single Pd atoms were obtained in the spectrum of Pd,$RuS_{2-x}O_y$, which again confirmed the atomic doping of Pd.

To ascertain the chemical environment of Pd atoms in Pd,$RuS_{2-x}O_y$, extended X-ray absorption fine structure (EXAFS) spectroscopy was conducted. Fourier transform (FT) of the k^3-weighted Pd K-edge EXAFS spectra (Fig. 3b, Fig. S4 and Table S1) for Pd,$RuS_{2-x}O_y$ shows the disappearance of the first-shell Pd–Pd scattering peak at 2.68 Å when compared with that of Pd foil, suggesting that the Pd species were not in the form of metallic Pd nanoparticles or clusters. Only Pd−S coordination existed in the first shell (R = 1.85 Å). Moreover, the fitting results of k^2-weighted Pd K-edge FT spectrum exhibits a similar profile and fitting parameters (Pd–S bond distance: 2.3 Å and CN: 4.3) to those of Ru (Ru–S bond distance: 2.25 Å and CN: 5.1) (Fig. 3c, Fig. S5 and Table S2), implying the substitution of Ru atoms by Pd atoms. In addition, the leaching of Ru ions into the final reactant solution was measured by inductively coupled plasma mass spectrometry (ICP–MS) (Table S3), further validating the substitution of Ru atoms by Pd atoms. ICP–MS and X-ray photoelectron spectroscopy (XPS) results verified the successful doping of Pd, with the Ru: Pd stoichiometries of 46: 1 and 13:1, respectively. A shorter scattering path was also observed in the Ru FT EXAFS spectra of Pd,$RuS_{2-x}O_y$. According to the best fitting results, the peak at 2.06 Å was satisfactorily interpreted as the scattering path of Ru–O, which might have formed owing to the incorporation of O sites via the doping of Pd (Fig. 3c and Table S2). O 1 s X-ray photoelectron spectrum of Pd,$RuS_{2-x}O_y$ was deconvoluted into three peaks corresponding to lattice O (M−O) (529.8 eV), O in physically adsorbed O_2 (O_{2ads}) (532.1 eV), and O in adsorbed water (H_2O_{ads}) (530.9 eV) (Fig. 3d) [22]. Furthermore, the XPS spectra demonstrated that the content of O sites increased with an increase in Pd doping content (Fig. S6), indicating the essential role of Pd in the introduction of O sites. In contrast, the XPS spectrum of RuS_2 did not show the peak of lattice O (Fig. S7). Furthermore, the PL spectrum also confirm the introduction of O sites is induced by the Pd doping. As shown in Fig. 3e, a strong PL emission was observed in the spectrum of pure RuS_2 because photoexcitation allowed radiative recombination. However, after Pd doping, the PL emission was remarkably reduced, suggesting severe oxidation or the formation of defects. To further identify the O-containing species in the catalysts, FT infrared (FTIR) spectroscopy was performed. To exclude the influence of H_2O_{ads}, Pd,$RuS_{2-x}O_y$ was pretreated under vacuum conditions to eliminate water from the sample. The spectrum of Pd, $RuS_{2-x}O_y$ showed the absence of the OH peak, further verifying that the O-containing surface species in Pd,$RuS_{2-x}O_y$ was O atoms (Fig. 3f). The abovementioned experimental observations confirm the spontaneous incorporation of O atoms into the RuS_2 backbone by Pd interfacial doping.

2.2. *Catalytic activity of the Pd,$RuS_{2-x}O_y$ model catalyst towards hydrogen evolution*

HER activities of all catalysts were analyzed in a N_2-saturated H_2SO_4 solution (0.5 M) using a standard three-electrode setup, and the state-of-the-art Pt/C catalyst was used for comparison. The measured polarization curves are shown in Fig. 4a-b. Pd,$RuS_{2-x}O_y$ exhibited higher HER activity than that of RuS_2, requiring the overpotentials of 38 and 82 mV to achieve the current densities of 10 and 100 mA cm^{-2}, respectively. Specifically, Pd,$RuS_{2-x}O_y$ showed even higher catalytic activity than that of Pt/C in the high current density region. To the best of our knowledge, the HER performance of Pd,$RuS_{2-x}O_y$ in acidic media is the highest among those of most of the PGM-free materials reported to date (see Table S4 for details) [4,5,11,16,23–25]. Compared with the current

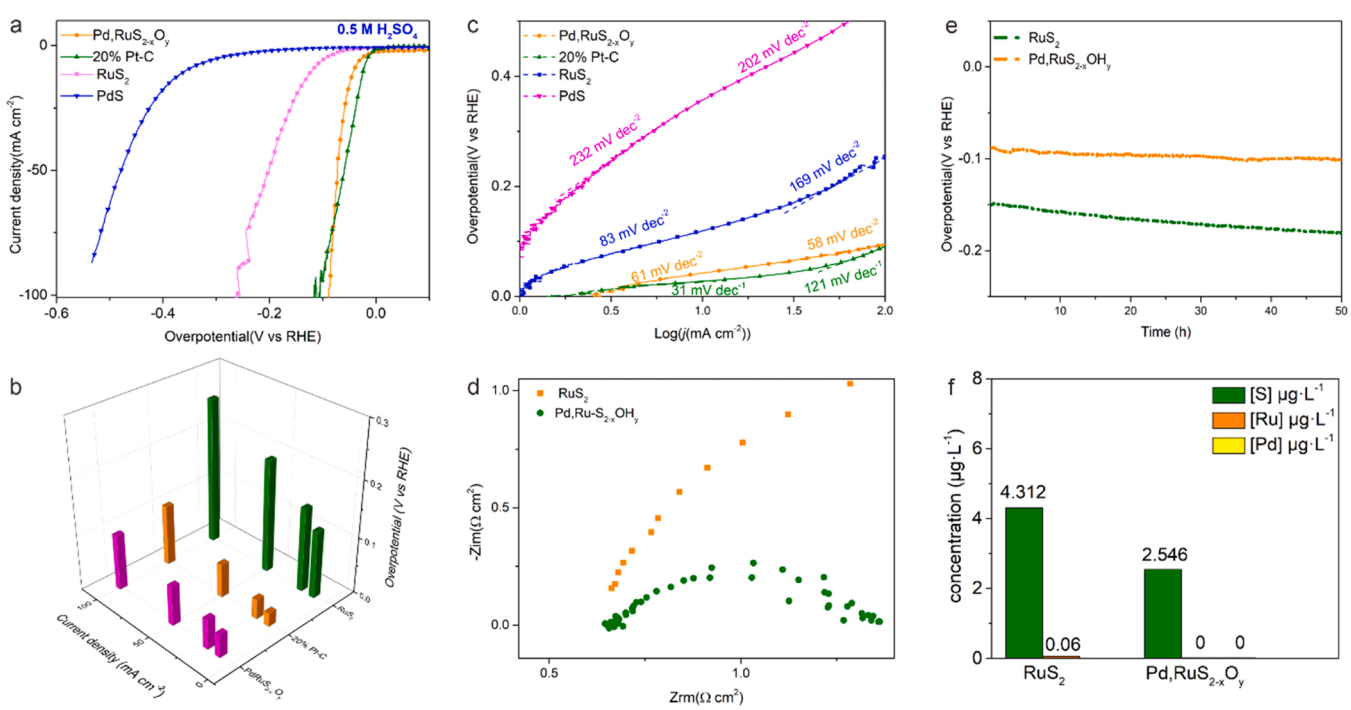

Fig. 4. (a) Linear sweep voltammetry polarization curves of Pd,$RuS_{2-x}O_y$, RuS_2, PdS, and 20 wt% Pt/C. (b) Comparison between the HER activities of Pd,$RuS_{2-x}O_y$, RuS_2, and 20 wt% Pt/C. (c) Tafel slopes of Pd,$RuS_{2-x}O_y$, RuS_2, and 20 wt% Pt/C. (d) Electrochemical impedance spectroscopy Nyquist plots for Pd,$RuS_{2-x}O_y$ and RuS_2. (e) Results of long-time operating stability tests. (f) Inductively coupled plasma optical emission spectra of the dissolved S, Ru, and Pd ions in the electrolyte after the stability tests.

densities of RuS_2 and Pd,$RuS_{2-x}O_y$, the current density of PdS was negligible, indicating that the electrocatalytic activity of Pd,$RuS_{2-x}O_y$ did not originate from the Pd sites. Additionally, Pd,$RuS_{2-x}O_y$ demonstrated less CO sensitivity (Fig. S8); this further excluded activity interference from Pd sites [19]. To further understand the origin of the differences in the overall catalytic performance between Pd,$RuS_{2-x}O_y$, and counterpart RuS_2 electrodes, we estimated the relative electrochemically active surface areas of these electrodes via cyclic voltammetry by calculating the double-layer capacitance (C_{dl}) at the solid−liquid interface (Fig. S9). The relative electrochemically active surface area of Pd,$RuS_{2-x}O_y$ was similar to that of RuS_2, suggesting that the higher catalytic performance of Pd,$RuS_{2-x}O_y$ was not owing to a larger surface area. Tafel slopes (Fig. 4c) can reflect the HER kinetics. In a low current density region (1–10 mA cm^{-2}), Pd,$RuS_{2-x}O_y$ demonstrated a lower Tafel slope (61 mV dec^{-1}) than that of RuS_2 (83 mV dec^{-1}), indicating that the kinetic radical step of HER process on Pd, $RuS_{2-x}O_y$ electrode. Especially, in high current density regions, the disparity is more evident. Moreover, the Tafel slope of Pd,$RuS_{2-x}O_y$ (58 mV dec^{-1}) was also obviously lower than that of 20 wt% Pt/C (121 mV dec^{-1}) at the same current density. This can be explained as follows: the current density in the low potential region was small, the reactant is sufficient. The HER at low potentials is mainly controlled by the thermodynamic behavior, and the dynamic behavior is not a key factor. However, at higher current density, mass transport plays a more important role. Considering that the role of O sites is to promote the dynamic behavior by facilitating H_3O^+ transfer, thus Pd,$RuS_{2-x}O_y$ shows much faster kinetic for HER. Additionally, electrochemical impedance spectroscopy (EIS) results also reveal that the electronic transport and mass transport resistances of Pd,$RuS_{2-x}O_y$ were significantly smaller than those of RuS_2, where the Nyquist plots (Fig. 4d) demonstrated a substantial reduction in charge transfer resistance (Rct) from 14.6 Ω cm^2 for RuS_2 to 0.67 Ω cm^2 for Pd,$RuS_{2-x}O_y$ (Fig. S10 and Table S5). Although the positive effect of O sites on the performance activation of RuS_2 was confirmed, the excessive increase in O concentration caused a decline in the performance of RuS_2 (Fig. S11).

The stability of HER electrocatalysts in acidic electrolytes is another critical factor to evaluate the performances of these electrocatalysts as S leaching occurs in corrosive electrolytes. Pd,$RuS_{2-x}O_y$ showed excellent long-term cycling stability, and no considerable potential decay was observed after 5000 cycles (Fig. S12). The excellent stability of Pd, $RuS_{2-x}O_y$ was further assessed by $\Delta\eta = \eta_{final} - \eta_{initial}$, where $\eta_{initial}$ and η_{final} represent the final and initial overpotentials, respectively, and Δη denotes the difference between $\eta_{initial}$ and η_{final}, which was determined via a chronopotentiometric test at 10 mA cm^{-2}. As shown in Fig. 4e, Pd, $RuS_{2-x}O_y$ showed highly durable stability beyond 50 h with an increase of only 12 mV in potential. In contrast, RuS_2 exhibited low operational stability with a large Δη of 38 mV. To confirm the fixation of S on Pd, $RuS_{2-x}O_y$, ex situ ICP–MS was performed to analyze the concentration of dissolved S in the test electrolyte during the 50 h stability test. ICP-MS results demonstrated a reduced S concentration (4.312 ppm versus 2.546 ppm) in the test electrolyte (Fig. 4f), which indicated that Pd, $RuS_{2-x}O_y$ was more stable than pristine RuS_2. Furthermore, no leaching of Ru and Pd in the electrolyte was noticed after the tests. XPS was employed to examine the valence state of Pd in Pd,$RuS_{2-x}O_y$ after electrolysis. Notably, neither the content nor the valence state of Pd in Pd,$RuS_{2-x}O_y$ was altered after the test according to the XPS results, suggesting that Pd was strongly doped into the RuS_2 lattice and was highly stable under working conditions (Fig. S13). The post-XPS results of Pd,$RuS_{2-x}O_y$ after electrolysis revealed that the O sites were also firmly integrated into the RuS_2 backbone and were highly stable under electrolytic conditions (Fig. S14). Therefore, in addition to having a high HER activity, Pd,$RuS_{2-x}O_y$ shows excellent HER stability.

2.3. Role of non-covalent hydrogen bonding interactions

Herein, we employed a combination of experimental and theoretical techniques to explore the role of non-covalent hydrogen bonding interactions in the performance enhancement of Pd,$RuS_{2-x}O_y$. Initially, we calculated the H adsorption free energy (ΔG_H) (Fig. S15-17), which was successfully used as a descriptor for predicting the catalytic activity of various sites. ΔG_H of the O sites in Pd,$RuS_{2-x}O_y$ are far from ideal, suggesting unfavorable H adsorption. Additionally, the adsorption energies of H on the Pd site and its adjacent S sites were also investigated, and the obtained values were also unsatisfactory [6]. Therefore, the increased catalytic behavior was not due to the regulation of the energetic interaction between reaction intermediates (H*) and the surface site. In other words, the increased HER performance was not attributed to the introduction of new active sites. Subsequently, DFT calculations were conducted to analyze the non-covalent interactions at electrode–liquid interfaces of Pd,$RuS_{2-x}O_y$ catalyst (Fig. 5a and Fig. S18-19)· H_2O stabilized the adsorption energy, which was lowered to approximately half on the S sites (−1.006 eV) as compared to that on the O sites (−2.059 eV) of Pd,$RuS_{2-x}O_y$; this implied that water molecules were significantly more likely to be absorbed on the O sites. Moreover, strong H-bonds with a very short O−H distance of 1.851 Å were noticed. Then, we evaluated the electron localization function (Fig. 5b) to provide a precise basis for the analysis of wave function and bonding between water molecules and O sites. The topological image shows that the V(O, H) basin belongs to the O sites in the Pd,$RuS_{2-x}O_y$ valence shell sharing a boundary with the V(O) basin, which is typical for hydrogen bonding [26–28]. To study the bonding and electronic structure between the O sites and H_2O, projected density of states (pDOS) analysis was executed. pDOS analysis results (Fig. S20a and Fig. S21a) demonstrated that the delocalized molecular orbitals of O adsorbed on Pd,$RuS_{2-x}O_y$ weakly interacted with the H 1 s orbital in the − 9.2—9.0 eV energy region, thus confirming the presence of non-covalent bonding. Additionally, we performed crystal orbital Hamilton population (COHP) analyses (Fig. 5c, Fig. S20b and Fig. S21b) based on the wave function obtained from periodic DFT calculations [29,30], which enabled the computation of the energetic bonding and antibonding contributions of orbital overlaps between molecules. The COHP value showed that the antibonding interactions (–COHP < 0) of H_2O adsorbed on the O sites were considerably stronger than the bonding (–COHP > 0) interactions, further implying hydrogen bonding interactions between H_2O and O sites [31]. To model the non-covalent hydrogen bonding interactions between the O sites and hydrated cations ($H^+(H_2O)_n$) located in the outer Helmholtz plane (OHP) in the real interfacial environment, we further used the double layer water to simulate the electrochemical double layer. Additionally, we also consider the charge-mediated interactions between the cation (hydrated cations, $H^+(H_2O)_n$) and the electrode surface. We then used DFT calculations to computed the interaction energies of $H^+(H_2O)_n$ and O sites. We found that the introduction of O sites increases the no-covalent interaction energies between hydrated cations (or water molecules) and electrode surface with respect to the case in which no O sites are present, and the interaction energies is larger in the presence of O sites that without O sites by 0.26∼ 0.59 eV per adsorbed O sites (Fig. 5d-f and Fig. S22-23). Furthermore, this change in interaction energies, which are less than 80 kJ mol per adsorbed O sites, further indicates that the interaction between O sites groups and adsorbed cations can be classified as non-covalent.

Bader charge analysis (Fig. 6a-b) is also useful for understanding the catalytic activity of the sites where non-covalent interactions play an important role [32–34]. Bader charge analysis results indicated a strong acceptor-type behavior of the O sites, characterized by almost four times higher electron affinity (−1.1604 e^-) than that of S atoms (−0.2944 e^-) [35]. The locally increased electron affinity can lead to localized negative charges on the O sites, which can substantially facilitate the adsorption of $H^+(H_2O)_n$ from the acidic electrolyte. The non-covalent interaction was also experimentally investigated by kinetic isotope effect (KIE) [36–40], contact angle, and the potential of zero charge (PZC) evaluations. The role of interfacial non-covalent interaction in the HER of Pd,$RuS_{2-x}O_y$ in aqueous electrolyte was examined via KIE studies by

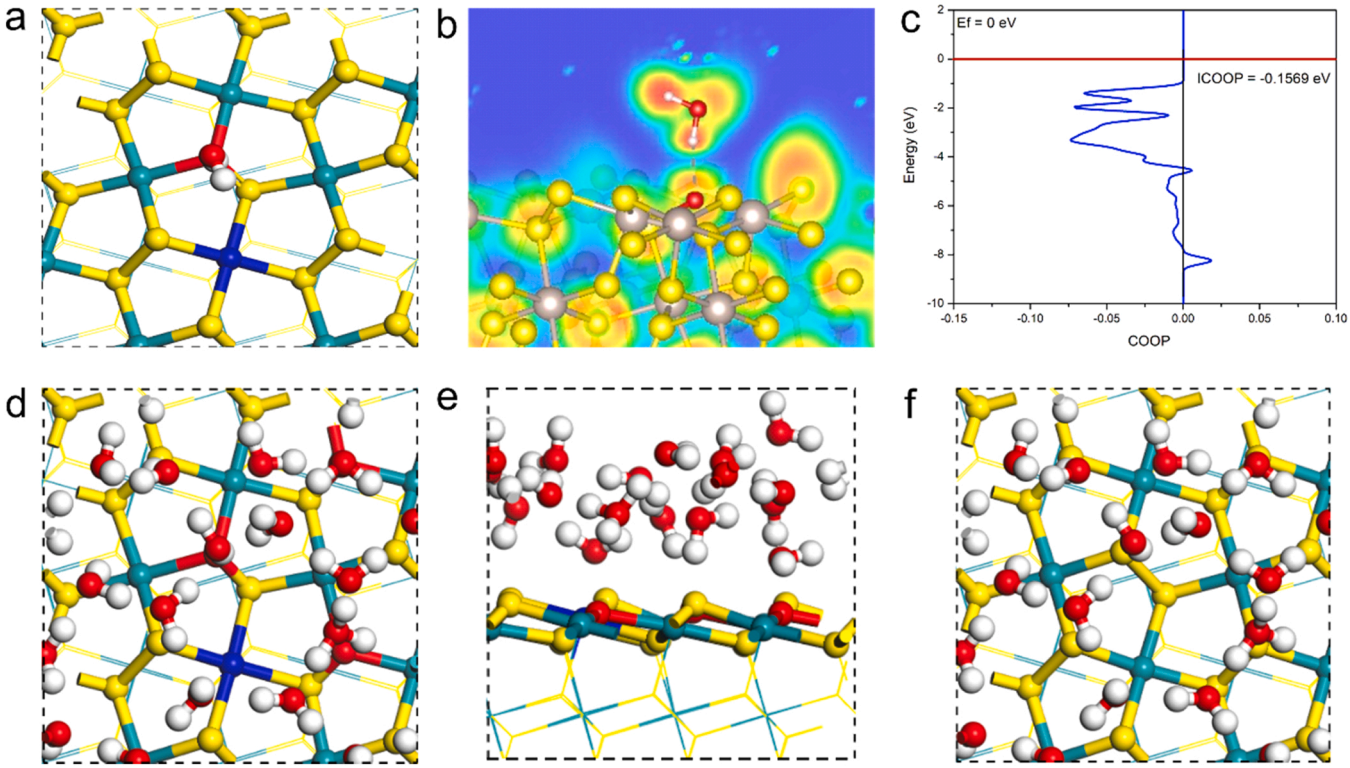

Fig. 5. (a) Interaction energy between H_2O and the O sites. (b) Electron localization function evaluation. (c) Crystal orbital Hamilton population bonding analysis results. (d) Interaction energy between H^+ $(H_2O)_n$ and the O sites on Pd,$RuS_{2-x}O_y$, $E_{ads} = -1.804554$ eV (Top view). (e) Interaction energy between H^+ $(H_2O)_n$ and the O sites on Pd,$RuS_{2-x}O_y$ (side view). (f) Interaction energy between $H^+(H_2O)_n$ and the S sites on RuS_2, $E_{ads} = -1.548834$ eV (Top view). Blue, red, white, light sea green and yellow balls indicate Pd, O, H, Ru and S atoms, respectively.

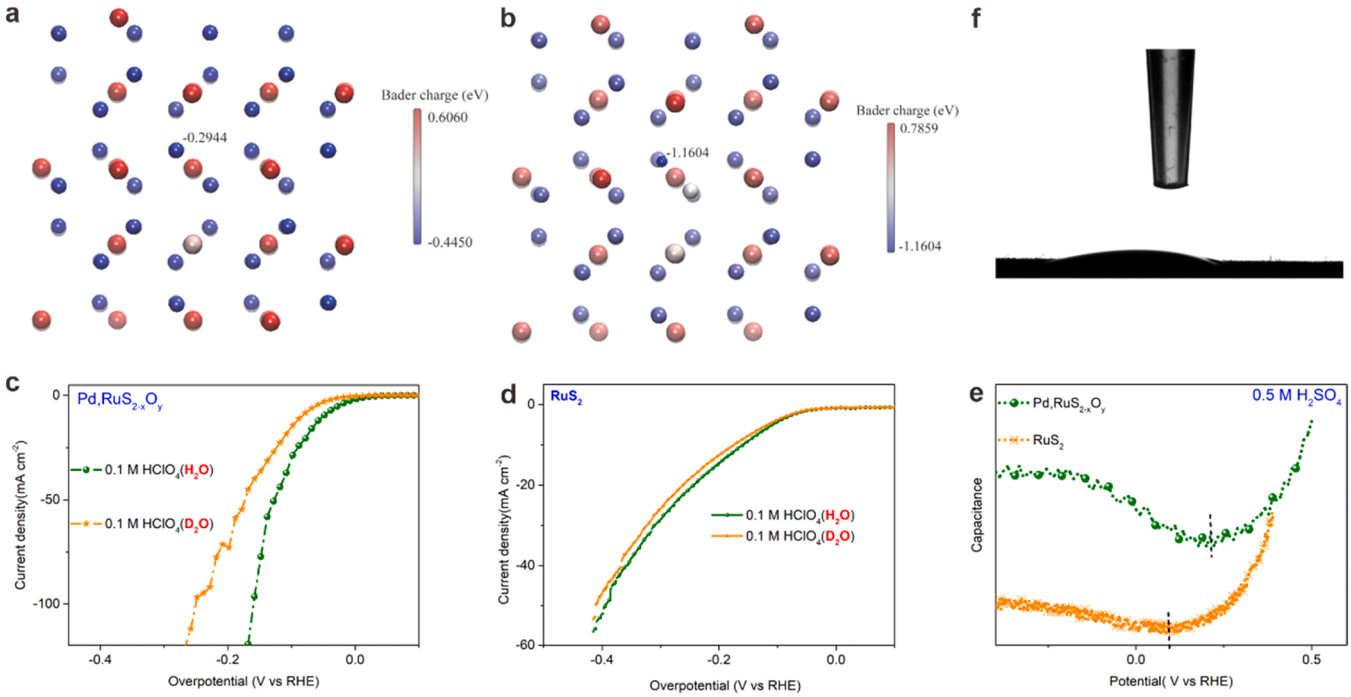

Fig. 6. (a-b) Bader charge analysis of the Pd,$RuS_{2-x}O_y$ surface revealing the electron acceptor nature of the O substitution site characterized by − 1.1604 e negative charge as compared to − 0.2944 e on the S atoms. Electron localization function evaluation. Blue, red, rosy and purple balls indicate O, Ru, Pd and S atoms, respectively. (c) HER polarization curves of the Pd,$RuS_{2-x}O_y$ electrode in N_2-saturated 0.1 M $HClO_4$ with H_2O or D_2O. (d) HER polarization curves of the RuS_2 electrode in N_2-saturated 0.1 M $HClO_4$ with H_2O or D_2O. (e) E_{PZC} measured for RuS_2 and Pd,$RuS_{2-x}O_y$. (f) contact angel of Pd,$RuS_{2-x}O_y$ (~12°).

substituting H_2O with D_2O in the electrolyte of 0.1 M $HClO_4$. We found that the substitution of H_2O with D_2O in the 0.1 M $HClO_4$ electrolyte markedly slowed the HER rate of Pd,$RuS_{2-x}O_y$ in an acidic environment, specifically in high current density regions (see Fig. 6c). These results indicate that the HER kinetic performance of Pd,$RuS_{2-x}O_y$ is not only governed by the energetic interaction between H and the surface site (ΔG_{H^*}), but also limited by the mass transport of reactants from the bulk electrolyte to the electrode. The O sites endows the interface with reactant dragging functionality, through forming strong non-covalent hydrogen bonding to the reactants. Thus, the slow diffusion of $D^+(D_2O)_n$ will affect the mass transport of the reactants from bulk electrolyte to electrode interface, thereby affecting its hydrogen evolution activity specifically in high current density regions [39]. By contrast, the HER kinetics of RuS_2 does not slow down significantly upon substitution of H_2O with D_2O since it is not limited by the diffusion of reactants from the bulk electrolyte to the electrode (Fig. 6d). Furthermore, this results also rule out the influence of other noncovalent interactions between water molecules (H_2O–H_2O) or between water and the supporting electrolyte cation (H^+–H_2O) toward HER kinetics. The result obtained above supports our claim that interfacial non-covalent interactions (H bonding) between $H^+(H_2O)_n$ and O sites increase the electrocatalytic activity of Pd,$RuS_{2-x}O_y$. The contact angle test offers a macroscopic proof [6], and the corresponding results imply that Pd,$RuS_{2-x}O_y$ exhibits stronger hydrophilicity than that of pure RuS_2 (Fig. 6e and Fig. S24). This is further reflected in the potential of zero charge (PZC) (Fig. 6f), where more polarized Pd,$RuS_{2-x}O_y$ represents a considerably more positive value at 0.245 V vs. reversible hydrogen electrode (RHE) than that of RuS_2 (0.102 V) [41]. The potential of zero charge of electrode is correlated with interfacial water reorganization energetics. Thus, the presence of O sites in Pd,$RuS_{2-x}O_y$ improves the HER kinetics as these sites form strong non-covalent H bonds with reactants, allowing a more efficient mass transfer through the double layer.

3. Conclusions

In summary, herein, using Pd,$RuS_{2-x}O_y$ as a model catalyst surface to decouple the effect of each interaction (ΔG_H, noncovalent interactions) on the HER kinetics, the importance of non-covalent interactions in the HER performance enhancement of catalysts was thus confirmed. We found that hydrated cations located in the outer Helmholtz plane (OHP) also interact directly with electrode materials and the strength of these interactions would tune the concentration of reactants on the surface interface. Owing to non-covalent interaction engineering, Pd,$RuS_{2-x}O_y$ exhibited remarkable electrocatalytic performance for HER with a significantly low overpotential of only 82 at a current density of 100 mA cm^{-2}, which is the highest performance among those of most of the state-of-the-art catalysts reported to date and even comparable to that of Pt/C. Beyond high catalytic activity, the Pd,$RuS_{2-x}O_y$ showed an outstanding long-term operational stability beyond 50 h with an observed potential increase of only 12 mV, rendering it a promising candidate for industrial application. Although the present paper has centered on the Pd,$RuS_{2-x}O_y$, the concepts and approaches presented in our study go well beyond this system, and should be extremely helpful to provide a new path for utilizing the electrocatalytic potential of Pt group metal-free catalysts for efficient hydrogen generation in acidic solutions.

Declaration of Competing Interest

There are no conflicts to declare.

Acknowledgements

This work was financially supported by the National Natural Science Foundation of China (22109100, 21671136), Guangdong Basic and Applied Basic Research Foundation (2020A1515010379), Shenzhen Science and Technology Project Program (JCYJ20190808144413257, JCYJ20190808145203535), Shenzhen Key Projects of Technological Research (JSGG20200925145800001) and Instrumental Analysis Center of Shenzhen University.

Author contributions

Z. L., X.R. and X. S. designed the project. Z.L. and L.W. contributed to the synthesis of material and the characterization. Z.L., L.W., X.S., X.R. and L.W. contributed to analysis of the electrochemical experiments results. Z.L. contributed to the theory calculation. H.Z and Z.J. contributed to the X-ray absorption fine structure spectroscopy. The manuscript was primarily written by Z.L., X.S. and X.R. All authors contributed to discussions and manuscript review.

Appendix A. Supporting information

Supplementary data associated with this article can be found in the online version at doi:10.1016/j.nanoen.2022.107654.

References

[1] J. Dai, Y. Zhu, H.A. Tahini, Q. Lin, Y. Chen, D. Guan, C. Zhou, Z. Hu, H.J. Lin, T. S. Chan, C.T. Chen, S.C. Smith, H. Wang, W. Zhou, Z. Shao, Single-phase perovskite oxide with super-exchange induced atomic-scale synergistic active centers enables ultrafast hydrogen evolution, Nat. Commun. 11 (1) (2020) 5657.
[2] N. Cheng, S. Stambula, D. Wang, M.N. Banis, J. Liu, A. Riese, B. Xiao, R. Li, T. K. Sham, L.M. Liu, G.A. Botton, X. Sun, Platinum single-atom and cluster catalysis of the hydrogen evolution reaction, Nat. Commun. 7 (2016) 13638.
[3] K. Jiang, M. Luo, M. Peng, Y. Yu, Y.R. Lu, T.S. Chan, P. Liu, F.M.F. de Groot, Y. Tan, Dynamic active-site generation of atomic iridium stabilized on nanoporous metal phosphides for water oxidation, Nat. Commun. 11 (1) (2020) 2701.
[4] W. Wu, C. Niu, C. Wei, Y. Jia, C. Li, Q. Xu, Activation of MoS2 basal planes for hydrogen evolution by zinc, Angew. Chem. Int. Ed. Engl. 58 (7) (2019) 2029–2033.
[5] X. Meng, C. Ma, L. Jiang, R. Si, X. Meng, Y. Tu, L. Yu, X. Bao, D. Deng, Distance synergy of MoS2 -confined rhodium atoms for highly efficient hydrogen evolution, Angew. Chem. Int. Ed. Engl. 59 (26) (2020) 10502–10507.
[6] K. Wu, K. Sun, S. Liu, W.-C. Cheong, Z. Chen, C. Zhang, Y. Pan, Y. Cheng, Z. Zhuang, X. Wei, Y. Wang, L. Zheng, Q. Zhang, D. Wang, Q. Peng, C. Chen, Y. Li, Atomically dispersed Ni–Ru–P interface sites for high-efficiency pH-universal electrocatalysis of hydrogen evolution, Nano Energy 80 (2021).
[7] I.T. McCrum, M.T.M. Koper, The role of adsorbed hydroxide in hydrogen evolution reaction kinetics on modified platinum, Nat. Energy (2020).
[8] Z. Luo, Y. Ouyang, H. Zhang, M. Xiao, J. Ge, Z. Jiang, J. Wang, D. Tang, X. Cao, C. Liu, W. Xing, Chemically activating MoS2 via spontaneous atomic palladium interfacial doping towards efficient hydrogen evolution, Nat. Commun. 9 (1) (2018) 2120.
[9] H. Li, M. Hu, L. Zhang, L. Huo, P. Jing, B. Liu, R. Gao, J. Zhang, B. Liu, Hybridization of bimetallic molybdenum-tungsten carbide with nitrogen-doped carbon: a rational design of super active porous composite nanowires with tailored electronic structure for boosting hydrogen evolution catalysis, Adv. Funct. Mater. (2020).
[10] H. Wang, X. Xiao, S. Liu, C.L. Chiang, X. Kuai, C.K. Peng, Y.C. Lin, X. Meng, J. Zhao, J. Choi, Y.G. Lin, J.M. Lee, L. Gao, Structural and electronic optimization of MoS2 edges for hydrogen evolution, J. Am. Chem. Soc. 141 (46) (2019) 18578–18584.
[11] Y. Yin, Y. Zhang, T. Gao, T. Yao, X. Zhang, J. Han, X. Wang, Z. Zhang, P. Xu, P. Zhang, X. Cao, B. Song, S. Jin, Synergistic phase and disorder engineering in 1T-MoSe2 nanosheets for enhanced hydrogen-evolution reaction, Adv. Mater. 29 (28) (2017).
[12] M.T.M. Koper, Activity volcanoes for the electrocatalysis of homolytic and heterolytic hydrogen evolution, J. Solid State Electrochem. 20 (4) (2015) 895–899.
[13] B. Pattengale, Y. Huang, X. Yan, S. Yang, S. Younan, W. Hu, Z. Li, S. Lee, X. Pan, J. Gu, J. Huang, Dynamic evolution and reversibility of single-atom Ni(II) active site in 1T-MoS2 electrocatalysts for hydrogen evolution, Nat. Commun. 11 (1) (2020).
[14] J. Ru, T. He, B. Chen, Y. Feng, L. Zu, Z. Wang, Q. Zhang, T. Hao, R. Meng, R. Che, C. Zhang, J. Yang, Covalent assembly of MoS2 nanosheets with SnS nanodots as linkages for lithium/sodium-ion batteries, Angew. Chem. Int. Ed. Engl. (2020).
[15] L. Zhai, T.W. Benedict Lo, Z.-L. Xu, J. Potter, J. Mo, X. Guo, C.C. Tang, S.C. Edman Tsang, S.P. Lau, In situ phase transformation on nickel-based selenides for enhanced hydrogen evolution reaction in alkaline medium, ACS Energy Lett. 5 (8) (2020) 2483–2491.
[16] Y. Zhou, J. Zhang, E. Song, J. Lin, J. Zhou, K. Suenaga, W. Zhou, Z. Liu, J. Liu, J. Lou, H.J. Fan, Enhanced performance of in-plane transition metal dichalcogenides monolayers by configuring local atomic structures, Nat. Commun. 11 (1) (2020) 2253.
[17] Y. Li, X. Tan, R.K. Hocking, X. Bo, H. Ren, B. Johannessen, S.C. Smith, C. Zhao, Implanting Ni-O-VOx sites into Cu-doped Ni for low-overpotential alkaline hydrogen evolution, Nat. Commun. 11 (1) (2020) 2720.

[18] B. Mao, P. Sun, Y. Jiang, T. Meng, D. Guo, J. Qin, M. Cao, Identifying the transfer kinetics of adsorbed hydroxyl as a descriptor of alkaline hydrogen evolution reaction, Angew. Chem. Int Ed. Engl. (2020).

[19] Z. Luo, H. Zhang, Y. Yang, X. Wang, Y. Li, Z. Jin, Z. Jiang, C. Liu, W. Xing, J. Ge, Reactant friendly hydrogen evolution interface based on di-anionic MoS2 surface, Nat. Commun. 11 (1) (2020) 1116.

[20] J. Peto, T. Ollar, P. Vancso, Z.I. Popov, G.Z. Magda, G. Dobrik, C. Hwang, P. B. Sorokin, L. Tapaszto, Spontaneous doping of the basal plane of MoS2 single layers through oxygen substitution under ambient conditions, Nat. Chem. 10 (12) (2018) 1246–1251.

[21] D. Han, Z. Luo, Y. Li, N. Gao, J. Ge, C. Liu, W. Xing, Synergistic engineering of MoS2 via dual-metal doping strategy towards hydrogen evolution reaction, Appl. Surf. Sci. 529 (2020).

[22] Y. Wang, Y. Yang, S. Jia, X. Wang, K. Lyu, Y. Peng, H. Zheng, X. Wei, H. Ren, L. Xiao, J. Wang, D.A. Muller, H.D. Abruna, B.J. Hwang, J. Lu, L. Zhuang, Synergistic Mn-Co catalyst outperforms Pt on high-rate oxygen reduction for alkaline polymer electrolyte fuel cells, Nat. Commun. 10 (1) (2019) 1506.

[23] K. Qi, X. Cui, L. Gu, S. Yu, X. Fan, M. Luo, S. Xu, N. Li, L. Zheng, Q. Zhang, J. Ma, Y. Gong, F. Lv, K. Wang, H. Huang, W. Zhang, S. Guo, W. Zheng, P. Liu, Single-atom cobalt array bound to distorted 1T MoS2 with ensemble effect for hydrogen evolution catalysis, Nat. Commun. 10 (1) (2019) 5231.

[24] J. Yu, Y. Guo, S. Miao, M. Ni, W. Zhou, Z. Shao, Spherical ruthenium disulfide-sulfur-doped graphene composite as an efficient hydrogen evolution electrocatalyst, ACS Appl. Mater. Interfaces 10 (40) (2018) 34098–34107.

[25] Z. Zheng, L. Yu, M. Gao, X. Chen, W. Zhou, C. Ma, L. Wu, J. Zhu, X. Meng, J. Hu, Y. Tu, S. Wu, J. Mao, Z. Tian, D. Deng, Boosting hydrogen evolution on MoS2 via co-confining selenium in surface and cobalt in inner layer, Nat. Commun. 11 (1) (2020) 3315.

[26] S.J. Grabowski, What is the covalency of hydrogen bonding? Chem. Rev. 111 (4) (2011) 2597–2625.

[27] R.S.J. Proctor, A.C. Colgan, R.J. Phipps, Exploiting attractive non-covalent interactions for the enantioselective catalysis of reactions involving radical intermediates, Nat. Chem. 12 (11) (2020) 1–15.

[28] Q. Yang, W. Xu, S. Gong, G. Zheng, Z. Tian, Y. Wen, L. Peng, L. Zhang, Z. Lu, L. Chen, Atomically dispersed Lewis acid sites boost 2-electron oxygen reduction activity of carbon-based catalysts, Nat. Commun. 11 (1) (2020) 5478.

[29] J. Ma, Q. Zhi, L. Gong, Y. Shen, D. Sun, Y. Guo, L. Zhang, Z. Xia, A universal descriptor based on pz-orbitals for the catalytic activity of multi-doped carbon bifunctional catalysts for oxygen reduction and evolution, Nanoscale 12 (37) (2020) 19375–19382.

[30] G. Papoian, J.K. Norskov, R. Hoffmann, A comparative theoretical study of the hydrogen, methyl, and ethyl chemisorption on the Pt(111) surface, J. Am. Chem. Soc. 122 (17) (2000) 4129–4144.

[31] M. Tachibana, K. Yoshizawa, A. Ogawa, H. Fujimoto, R. Hoffmann, Sulfur-gold orbital interactions which determine the structure of alkanethiolate/Au(111) self-assembled monolayer systems, J. Phys. Chem. B 106 (49) (2002) 12727–12736.

[32] J.H. Zagal, M.T. Koper, Reactivity descriptors for the activity of molecular MN4 catalysts for the oxygen reduction reaction, Angew. Chem. Int. Ed. Engl. 55 (47) (2016) 14510–14521.

[33] J. Peto, T. Ollar, P. Vancso, Z.I. Popov, G.Z. Magda, G. Dobrik, C.Y. Hwang, P. B. Sorokin, L. Tapaszto, Spontaneous doping of the basal plane of MoS2 single layers through oxygen substitution under ambient conditions, Nat. Chem. 10 (12) (2018) 1246–1251.

[34] M. He, C. Li, H. Zhang, X. Chang, J.G. Chen, W.A. Goddard 3rd, M.J. Cheng, B. Xu, Q. Lu, Oxygen induced promotion of electrochemical reduction of CO_2 via co-electrolysis, Nat. Commun. 11 (1) (2020) 3844.

[35] Y. Zhou, F. Che, M. Liu, C. Zou, Z. Liang, P. De Luna, H. Yuan, J. Li, Z. Wang, H. Xie, H. Li, P. Chen, E. Bladt, R. Quintero-Bermudez, T.-K. Sham, S. Bals, J. Hofkens, D. Sinton, G. Chen, E.H. Sargent, Dopant-induced electron localization drives CO_2 reduction to C2 hydrocarbons, Nat. Chem. 10 (9) (2018) 974–980.

[36] X. Zhao, T. Gunji, T. Kaneko, Y. Yoshida, S. Takao, K. Higashi, T. Uruga, W. He, J. Liu, Z. Zou, An integrated single-electrode method reveals the template roles of atomic steps: disturb interfacial water networks and thus affect the reactivity of electrocatalysts, J. Am. Chem. Soc. 141 (21) (2019) 8516–8526.

[37] T.Y. George, T. Asset, A. Avid, P. Atanassov, I.V. Zenyuk, Kinetic isotope effect as a tool to investigate the oxygen reduction reaction on Pt-based electrocatalysts - Part I: high-loading Pt/C and Pt extended surface, Chemphyschem 21 (6) (2020) 469–475.

[38] S. Yu, P.K. Jain, Isotope effects in plasmonic photosynthesis, Angew. Chem. Int. Ed. Engl. (2020).

[39] E. Liu, L. Jiao, J. Li, T. Stracensky, Q. Sun, S. Mukerjee, Q. Jia, Interfacial water shuffling the intermediates of hydrogen oxidation and evolution reactions in aqueous media, Energy Environ. Sci. (2020).

[40] S. Kannath, P. Adamczyk, D. Ferro-Costas, A. Fernandez-Ramos, D.T. Major, A. Dybala-Defratyka, Role of microsolvation and quantum effects in the accurate prediction of kinetic isotope effects: the case of hydrogen atom abstraction in ethanol by atomic hydrogen in aqueous solution, J. Chem. Theory Comput. 16 (2) (2020) 847–859.

[41] C.H. Choi, H.-K. Lim, M.W. Chung, G. Chon, N. Ranjbar Sahraie, A. Altin, M.-T. Sougrati, L. Stievano, H.S. Oh, E.S. Park, F. Luo, P. Strasser, G. Dražić, K.J. J. Mayrhofer, H. Kim, F. Jaouen, The Achilles' heel of iron-based catalysts during oxygen reduction in an acidic medium, Energy Environ. Sci. 11 (11) (2018) 3176–3182.

Zhaoyan Luo received her PhD degree in Nanomaterial Chemistry (2019) from University of Science and Technology of China with Prof. Wei Xing. She is currently a postdoctoral associate with Professor Xiangzhong Ren@ Lei Wang at Shenzhen University. Her research interests include the controlled synthesis and characterization of two-dimensional (2D) materials (transition metal dichalcogenides, MXene) and carbon materials (graphene and CNTs) as well as their applications in catalysis (photocatalysis), energy storage and conversion (fuel cell, lithium-ion battery and supercapacitor).

Lei Zhang received his BS degree in Chemistry (2008) and PhD degree in Nanomaterial Chemistry (2014) from Xiamen University with Prof. Zhaoxiong Xie. He was a visiting graduate student at Georgia Institute of Technology in Prof. Younan Xia's group from 2012 to 2014. From 2015–2016, he worked as a Postdoc at Collaborative Innovation Center of Chemical Science and Engineering at Tianjin University. He is currently a postdoctoral associate with Professor Xueliang Sun at University of Western Ontario. His research interests include the design and synthesis of metal nanomaterials and single atom catalysts for fuel cells, carbon dioxide reduction, and water splitting devices.

Lei Wu received the bachelor's degree from Southwest University of Science and Technology, China. He is currently a postgraduate with Professor Xiangzhong Ren at Shenzhen University. His research interests include the design and synthesis of two-dimensional materials and single atom catalysts for fuel cells, carbon dioxide reduction, and water splitting devices.

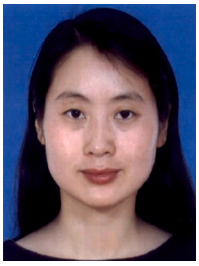

Qianling Zhang is a professor of College of Chemistry and Environmental Engineering in Shenzhen University, she received her PhD in inorganic chemistry in 2001 from Sun Yat-Sen University and then she joined Shenzhen University. Her current research interests are focus on the graphene-based materials for electrochemical energy storage and conversion, including electrocatalysis and electrodes in metal-air batteries and lithium-ion batteries.

Lei Wang received his PhD degree from Guangzhou Institute of Chemistry, Chinese Academy of Sciences. He was appointed as a full professor at college of Materials Science and Engineering in Shenzhen University, China in 2011. His research interests include the design and synthesis of novel butterfly-shaped organic semiconductor and single-walled carbon nanotube composites for high performance thermoelectric generators.

Xiangzhong Ren received the master degree from National University of Defense Technology, China in 1998 and the Ph.D. degree from Sichuan University, China in 2007. He was appointed as a full professor at college of Chemistry and Environmental Engineering in Shenzhen University, China in 2009. His research interests include the cathode and anode materials of lithium-ion batteries, nanocatalysts of metal-air battery, nanocomposites, and their related properties.

Prof. Xueliang (Andy) Sun is a Canada Research Chair in Development of Nanomaterials for Clean Energy, Fellow of the Royal Society of Canada and Canadian Academy of Engineering and Full Professor at the University of Western Ontario, Canada. Dr Sun received his PhD in materials chemistry in 1999 from the University of Manchester, UK, which he followed up by working as a postdoctoral fellow at the University of British Columbia, Canada and as a Research Associate at L'Institut National de la Recherche Scientifique (INRS), Canada. His current research interests are focused on advanced materials for electrochemical energy storage and conversion, including electrocatalysis in fuel cells and electrodes in lithium-ion batteries and metal–air batteries.